Models for randomly distributed nanoscopic domains on spherical vesicles

Vinicius N. P. Anghel,[1,*] Dima Bolmatov,[2,3,†] and John Katsaras[2,3,4,5,‡]

[1]*Nuclear Engineering and Systems Division, Canadian Nuclear Laboratories, Plant Road, Chalk River, Ontario, Canada K0J 1J0*

[2]*Neutron Scattering Division, Oak Ridge National Laboratory, P.O. Box 2008, Oak Ridge, Tennessee 37831-6453, USA*

[3]*Department of Physics and Astronomy, University of Tennessee, Knoxville, Tennessee 37996, USA*

[4]*Shull Wollan Center, Oak Ridge National Laboratory, P.O. Box 2008, Oak Ridge, Tennessee 37831-6453, USA*

[5]*Department of Physics, Brock University, 500 Glendale Avenue, St. Catharines, Ontario, Canada L2S 3A1*

(Received 9 February 2018; published 11 June 2018)

The existence of lipid domains in the plasma membrane of biological systems has proven controversial, primarily due to their nanoscopic size—a length scale difficult to interrogate with most commonly used experimental techniques. Scattering techniques have recently proven capable of studying nanoscopic lipid domains populating spherical vesicles. However, the development of analytical methods able of predicting and analyzing domain pair correlations from such experiments has not kept pace. Here, we developed models for the random distribution of monodisperse, circular nanoscopic domains averaged on the surface of a spherical vesicle. Specifically, the models take into account (i) intradomain correlations corresponding to form factors and interdomain correlations corresponding to pair distribution functions, and (ii) the analytical computation of interdomain correlations for cases of two and three domains on a spherical vesicle. In the case of more than three domains, these correlations are treated either by Monte Carlo simulations or by spherical analogs of the Ornstein-Zernike and Percus-Yevick (PY) equations. Importantly, the spherical analog of the PY equation works best in the case of nanoscopic size domains, a length scale that is mostly inaccessible by experimental approaches such as, for example, fluorescent techniques and optical microscopies. The analytical form factors and structure factors of nanoscopic domains populating a spherical vesicle provide a new and important framework for the quantitative analysis of experimental data from commonly studied phase-separated vesicles used in a wide range of biophysical studies.

DOI: 10.1103/PhysRevE.97.062405

I. INTRODUCTION

Biological membranes are composed mainly of lipids and proteins and are populated with substructures ranging in size from microns to nanometers. For instance, lipid domains (also known as lipid rafts when they contain proteins) exist as distinct, ordered regions in biological membranes [1–5]. Domains play an important physiological role in membrane function and have been implicated in protein and receptor trafficking, neurotransmission regulation, and signal transduction [6–11]. However, because biological membranes are highly complex assemblies, gaining physical insights into their nanoscopic domain structures and cross correlations has proven difficult, especially with regard to any analytical description [12–21]. Lipid domains and inclusions (e.g., proteins with circular symmetry) are commonly observed in lipid model membrane studies. Predicting the size and morphology of randomly distributed nanoscopic domains currently represents a computational challenge. Specifically, from a computational point of view, randomly distributed domains with circular symmetry on a spherical vesicle surface possess two main structural features to consider: (i) intradomain correlations, which in terms of scattering theory give rise to a form factor, and (ii) interdomain correlations, which can be derived from pair distribution functions (PDFs).

In this work, we present models describing the scattering from spherical vesicles with circular domains through an analytical approximation of their form factors and PDFs. Specifically, we describe the case of (i) "variable thickness spanning domains," i.e., domains whose thickness varies up to a maximum thickness corresponding to the thickness of the lipid bilayer (herein termed "fully spanning domains") [Fig. 1(a)], and (ii) "protruding domains" that extend beyond the bilayer. These domains can be either "half protruding" [Fig. 1(b)] or "fully protruding" [Fig. 1(c)].

The exact analytical computation of interdomain correlations for cases of two and three domains with circular symmetry on a spherical vesicle is analyzed in detail. The newly developed models for the random distribution of monodisperse nanoscopic domains averaged on the surface of a spherical vesicle extend the results from a previous work [22]. The Percus-Yevick (PY) equation in conjunction with the Ornstein-Zernike (OZ) compressibility relation has proven a powerful theoretical framework used in describing various complex fluids. In the case where the number of domains is greater than three, we developed an analytical approximation based on spherical analogs of the OZ and PY equations – in addition to a newly developed Monte Carlo (MC) algorithm. Importantly, the spherical analog of the OZ and PY equations works best for the description of nanoscopic domains, a length scale that

*Corresponding author: vinicius.anghel@cnl.ca

†Corresponding author: d.bolmatov@gmail.com

‡Corresponding author: katsarasj@ornl.gov

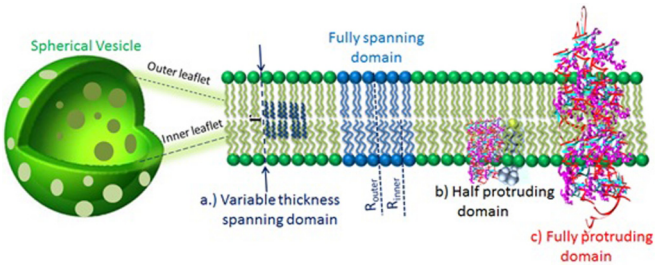

FIG. 1. A cross section of a spherical vesicle populated with the different domains and inclusions. The vesicle's lipid bilayer (i.e., thickness) is made of two lipid leaflets or monolayers (inner and outer). The lipid bilayer acts as a selective barrier and may also contain inclusions such as proteins or cholesterol-rich domains.

is mostly inaccessible by most currently used experimental techniques such as, for example, fluorescent techniques and optical microscopies.

In summary, we present models describing the scattering from spherical vesicles with circular domains suitable for analyzing neutron and x-ray scattering data. Analytical and semianalytical models were derived for scattering from monodisperse, circular domains on a vesicle. The analytical solution involves an expansion of the macroscopic optical potential in spherical harmonics, which results in a form factor that is an infinite sum over spherical harmonic orders, and which accounts for series truncation effects.

II. METHODS

Analysis of the structure and morphology of randomly distributed nanoscopic domains on spherical vesicles will enable experiments that will provide understanding at the molecular level. Scattering techniques are now commonly used to determine the structure of phase-separated membranes and their inclusions. However, there are currently no analytical models that can interpret the data from systems with more than one domain on the surface of a spherical vesicle.

Here, we introduce mathematical expressions describing the homogeneous and heterogeneous contributions to the scattering intensity. The general form of the scattering intensity can be written as

$$I(\boldsymbol{q}) = \frac{1}{4\pi}\int F(\boldsymbol{q})F(\boldsymbol{q})^* d\hat{q}, \tag{1}$$

where $F(\boldsymbol{q})$ is the scattering amplitude in the Born approximation:

$$F(\boldsymbol{q}) = -\int \rho(\boldsymbol{r})e^{-i\boldsymbol{q}\cdot\boldsymbol{r}}d^3\boldsymbol{r}, \tag{2}$$

where $\boldsymbol{r}$ is a vector from the origin to a point within the scattering object, $\boldsymbol{q}$ is a vector from the origin to the detector, and $\rho(\boldsymbol{r})$ is the coherent scattering length density (SLD).

A. Plane wave expansion and scattering length density

In this section we develop the notion of the SLD using the plane wave expansion. Any plane wave can be expanded as follows:

$$e^{-i\boldsymbol{q}\cdot\boldsymbol{r}} = 4\pi\sum_{l,m}(-i)^l j_l(qr)Y_l^m(\hat{q})Y_l^{m*}(\hat{r}), \tag{3}$$

where Y_l^m are spherical harmonics of degree l and orders m, and j_l are spherical Bessel functions of degree l. The coherent SLD $\rho(\boldsymbol{r})$ can be presented as a sum of the homogeneous contribution $\mu(r)$ with respect to angles θ and φ,

$$\mu(\boldsymbol{r}) = \mu(r) = \rho_c(r) - \rho_m, \tag{4}$$

and the heterogeneous contribution $\omega(\boldsymbol{r})$,

$$\omega(\boldsymbol{r}) = \begin{cases}\rho_d(r,\theta,\varphi) - \rho_c(r), & (\theta,\varphi)_{\text{in}},\\ 0, & (\theta,\varphi)_{\text{out}},\end{cases} \tag{5}$$

where ρ_c is the uniformly distributed continuous SLD within each phase, ρ_m is the SLD of a shell of uniform thickness suspended in an aqueous medium, ρ_d is the SLD of one or more circular domains within a shell, subscripts d and c refer, respectively, to the domain and continuous phases, and subscripts *in* and *out* refer, respectively, to positions inside and outside of a domain. Finally, we define the expansion coefficients of the heterogeneous contribution to the SLD $\omega(\boldsymbol{r})$ as

$$w_l^m(r) = \int \omega(\boldsymbol{r})Y_l^{m*}(\hat{r})d\hat{r}. \tag{6}$$

B. The homogeneous contribution

Here, we define the homogeneous radial SLD profile for a single spherical shell with inner and outer radii, R_i and R_o, respectively, as

$$\mu(r) = \begin{cases}0, & r < R_i\\ \rho_c - \rho_m, & R_i \leqslant r \leqslant R_o\\ 0, & r > R_o\end{cases}. \tag{7}$$

The Fourier transform of the homogenous radial SLD can be written as

$$\begin{aligned}&\int \mu(r)e^{-i\boldsymbol{q}\cdot\boldsymbol{r}}d^3\boldsymbol{r}\\ &= 4\pi\left(Y_0^0(\hat{q})\int_0^\infty \mu(r)r^2 j_0(qr)dr\int Y_0^{0*}(\hat{r})d\hat{r}\right)\\ &= 4\pi\left(2\sqrt{\pi}Y_0^0(\hat{q})M_0(q)\right),\end{aligned} \tag{8}$$

where

$$\begin{aligned}M_0(q) &= \int_0^\infty \mu(r)r^2 j_0(qr)dr\\ &= \frac{(\rho_c-\rho_m)}{q}\left[r^2\left(\frac{\sin qr}{(qr)^2} - \frac{\cos qr}{qr}\right)\right]\Bigg|_{R_i}^{R_o}.\end{aligned} \tag{9}$$

C. The heterogeneous contribution

The heterogeneous contribution to the SLD [Eq. (5)] can be expressed as a product of radial- and angular-dependent terms, such that $\omega(\boldsymbol{r}) = \omega(r)\tilde{\omega}(\hat{r})$, where

$$\omega(r) = \begin{cases}0, & r < R_i\\ \rho_d - \rho_c, & R_i \leqslant r \leqslant R_o\\ 0, & r > R_o\end{cases}, \tag{10}$$

$$\tilde{\omega}(\hat{r}) = \tilde{\omega}(\theta,\varphi) = \begin{cases}1, & 0 \leqslant \theta \leqslant \alpha_d\\ 0, & \alpha_d < \theta < \pi\end{cases}, \tag{11}$$

and where α_d in Eq. (11) is the angular size of a domain. Equation (11), therefore, represents the normalized angular SLD profile of a vesicle and, when substituted into Eq. (6), results in the normalized expansion coefficients:

$$\tilde{w}_l^m(\alpha_d) = \int \tilde{\omega}(\hat{r}) Y_l^{m*}(\hat{r}) d\hat{r} = \int_0^{2\pi} d\varphi \int_0^{\alpha_d} Y_l^{m*}(\theta,\varphi) \sin\theta \, d\theta. \tag{12}$$

The heterogeneous form factor can then be written as

$$\int \omega(\boldsymbol{r}) e^{-i\boldsymbol{q}\cdot\boldsymbol{r}} d^3\boldsymbol{r} = 4\pi \sum_{l,m} (-i)^l Y_l^m(\hat{q}) \tilde{w}_l^m(\alpha_d) W_l(q), \tag{13}$$

which contains the radial contribution namely,

$$W_l(q) = \int_0^\infty \omega(r) r^2 j_l(qr) dr. \tag{14}$$

III. RESULTS

A. Averaging over all domain positions

For all cases discussed in this section, the density of each domain is the product of angular- and radial-dependent factors, and the domains interact via a hard-core potential. This means that two domains can come into contact without changing their shape and cannot overlap each other. The scattered intensity can be written as [22]

$$\begin{aligned} I(\boldsymbol{q}) = 4\pi & \left[2\sqrt{\pi} M_0(q) + \sum_J \tilde{w}_0(\alpha_{d,J}) W_{0,J}(q) \right]^2 \\ & + 4\pi \sum_J \sum_{l=1}^\infty \left| \tilde{w}_{l,J}^0(\alpha_{d,J}) \right|^2 |W_{l,J}(q)|^2 \\ & + 4\pi \sum_{J\neq K} \sum_{l=1}^\infty \langle \tilde{\boldsymbol{w}}_{l,J}'^*(\alpha_{d,J}), \tilde{\boldsymbol{w}}_{l,K}'(\alpha_{d,K}) \rangle W_{l,J}(q) W_{l,K}(q). \end{aligned} \tag{15}$$

(The notation used in [22] is defined in the Methods section). This expression can be generalized further by considering that the angular and radial terms do not factor out. The form factor, $F(\boldsymbol{q})$, for the SLD $\rho(\boldsymbol{r}) = \mu(\boldsymbol{r}) + \omega(\boldsymbol{r})$ (see Methods and [22]) can be rewritten as

$$\begin{aligned} F(\boldsymbol{q};\boldsymbol{P}) &= -\int [\mu(\boldsymbol{r}) + \omega(\boldsymbol{r})] e^{-i\boldsymbol{q}\cdot\boldsymbol{r}} d^3\boldsymbol{r} \\ &= -4\pi (Y_0^0(\hat{q}) \int_0^\infty r^2 j_0(qr) dr \int \mu(r\hat{r}) Y_0^{0*}(\hat{r}) d\hat{r} \\ &\quad + \sum_{l,m} (-i)^l Y_l^m(\hat{q}) \int_0^\infty r^2 j_l(qr) w_l^m(r) dr), \end{aligned} \tag{16}$$

where $w_l^m(r)$ are the radially dependent expansion coefficients of the homogeneous SLD $\mu(\boldsymbol{r})$ in spherical harmonics, which has its center of gravity at a point $\boldsymbol{P}$.

One can thus rewrite the scattering intensity $I(\boldsymbol{q})$ as

$$\begin{aligned} I(\boldsymbol{q}) = 4\pi & \left[2\sqrt{\pi} M_0(q) + \sum_J \tilde{W}_0(\alpha_{d,J}, q) \right]^2 \\ & + 4\pi \sum_J \sum_{l=1}^\infty \langle \tilde{\boldsymbol{W}}_{l,J}'^*(\alpha_{d,J}, q; \boldsymbol{P}_J), \tilde{\boldsymbol{W}}_{l,J}'(\alpha_{d,J}, q; \boldsymbol{P}_J) \rangle \\ & + 4\pi \sum_{J\neq K} \sum_{l=1}^\infty \langle \tilde{\boldsymbol{W}}_{l,J}'^*(\alpha_{d,J}, q; \boldsymbol{P}_J), \tilde{\boldsymbol{W}}_{l,K}'(\alpha_{d,K}, q; \boldsymbol{P}_K) \rangle, \end{aligned} \tag{17}$$

where the components of the arrays $\tilde{\boldsymbol{W}}_{l,K}'$ are given by

$$\tilde{W}_{l,J}'^m(\alpha_{d,J}, q) = \int_0^\infty r^2 j_l(qr) w_l^m(r) dr. \tag{18}$$

Although this expression looks complicated, Eq. (17) has the advantage of simplifying the averaging process. To prepare for this process, we notice that there are terms for individual and pairs of domains. Since they cannot be treated the same, Eq. (17) is rewritten as

$$\begin{aligned} I(\boldsymbol{q}) = (4\pi)^2 |M_0(q)|^2 & + 2(4\pi)^{3/2} M_0(q) \sum_J \tilde{W}_0(\alpha_{d,J}, q) \\ & + 4\pi \sum_J \sum_{l=0}^\infty \langle \tilde{\boldsymbol{W}}_{l,J}'^*(\alpha_{d,J}, q), \tilde{\boldsymbol{W}}_{l,J}'(\alpha_{d,J}, q) \rangle \\ & + 4\pi \sum_{J\neq K} \sum_{l=1}^\infty \langle \tilde{\boldsymbol{W}}_{l,J}'^*(\alpha_{d,J}, q; \boldsymbol{P}_J), \tilde{\boldsymbol{W}}_{l,K}'(\alpha_{d,K}, q; \boldsymbol{P}_K) \rangle. \end{aligned} \tag{19}$$

The first term does not include domains, and the next two terms involve only individual domains. In this case, the scalar product does not depend on $\boldsymbol{P}_J$, because the scalar products $\langle \tilde{\boldsymbol{W}}_{l,J}'^*(\alpha_{d,J}, q), \tilde{\boldsymbol{W}}_{l,J}'(\alpha_{d,J}, q) \rangle$ do not depend on the position of the domain on the vesicle surface, only on domain shape. For these terms, all $\boldsymbol{P}_J$ dependencies can be dropped, and we assume that all domains are located at the vesicle's north pole.

The PDF of a domain center residing somewhere on the vesicle is constant. Moreover, being a PDF, its integral is unity; hence, the integration over angular coordinates for the first three terms of Eq. (19), is unity. The last term in Eq. (19) involves a pair of domains, or the probability distribution of two independent domains on a spherical surface. In this case, one can imagine distributions such as the following:

(a) The domains are not densely packed on the vesicle surface and one can therefore assume that their total relative area is negligible; i.e., they behave similar to a dilute gas.

(b) The domains are in close proximity to each other and behave like a dense gas or as liquid-like particles.

(c) The domains are densely packed and are expected to arrange themselves in a manner similar to atoms in a solid.

Since there is only a finite number of domains on a vesicle, there is no phase transition taking place between these different arrangements of domains on a spherical vesicle. This holds true only if there is no "domain reservoir/bath" that can add or remove domains from a vesicle.

1. An arbitrary number of randomly distributed domains

For an arbitrary number of randomly distributed domains we compute the average for a pair of domains $J \neq K$. Terms to be averaged are included in the scalar products and

expressed as

$$\langle \tilde{\boldsymbol{W}}^{'*}_{l,J}(\alpha_{d,J},q;\boldsymbol{P}_J),\tilde{\boldsymbol{W}}'_{l,K}(\alpha_{d,K},q;\boldsymbol{P}_K)\rangle. \quad (20)$$

It should be noted that any rigid rotation does not alter this scalar product. For the case $l=0$, the product $\tilde{W}_0(\alpha_{d,J})\tilde{W}_0(\alpha_{d,K})$ remains constant as it depends only on the relative positions of the domains and is described by three Euler angles: $(\alpha_{J,K},\beta_{J,K},\gamma_{J,K})$. Since the scalar product is invariant for the different rotations, one can drop the $\boldsymbol{P}_J$ dependence by using the transformation for the arrays $\tilde{\boldsymbol{W}}'_{l,K}$ as a result of rotational symmetry, or:

$$\begin{aligned}&\langle \tilde{\boldsymbol{W}}^{'*}_{l,J}(\alpha_{d,J},q;\boldsymbol{P}_J),\tilde{\boldsymbol{W}}'_{l,K}(\alpha_{d,K},q;\boldsymbol{P}_K)\rangle\\ &\quad=\langle \tilde{\boldsymbol{W}}^{*}_{l,J}(\alpha_{d,J}),\ \boldsymbol{D}_{l,\ J\to K}\tilde{\boldsymbol{W}}_{l,K}(\alpha_{d,K})\rangle, \end{aligned}\quad (21)$$

where $\boldsymbol{D}_{l,\ J\to K}$ is the matrix of Wigner $D^{m,m'}_{l;\ J,K}$ functions corresponding to harmonics of order l—associated with rotation—where the domain K is relocated from the sphere's north pole to a new position relative to domain J [22]. The arrays $\tilde{\boldsymbol{W}}^{*}_{l,J}(\alpha_{d,J})$ are all considered as above (i.e., located at the north pole), since the dependencies of $\boldsymbol{P}_J$ and $\boldsymbol{P}_K$ are included in the Wigner matrix $\boldsymbol{D}_{l,\ J\to K}$.

The probability distribution for the position of domain K relative to domain J depends on the angles $(\alpha_{J,K},\beta_{J,K},\gamma_{J,K})$, as was shown previously in [22]. The Wigner functions $D^{m,m'}_{l}(\alpha,\beta,\gamma)$ suffice in describing all rotations, as any function defined over the rotation group can be expressed as a linear combination of Wigner functions. Thus, the probability density, $(\alpha_{J,K},\beta_{J,K},\gamma_{J,K})$, or the probability of finding domain K at a position $(\alpha_{J,K},\beta_{J,K},\gamma_{J,K})$ relative to domain J, can be written as

$$\begin{aligned}&C(\alpha_{J,K},\beta_{J,K},\gamma_{J,K})\\ &\quad=\sum_{l=0}^{\infty}\sum_{m=-l}^{m=l}\sum_{m'=-l}^{m'=l}D^{m,m'}_{l}(\alpha_{J,K},\beta_{J,K},\gamma_{J,K})c^{m,m'}_{l}. \end{aligned}\quad (22)$$

The average for $\langle \tilde{\boldsymbol{W}}^{*}_{l,J}(\alpha_{d,J}),\ \boldsymbol{D}_{l,\ J\to K}\tilde{\boldsymbol{W}}_{l,K}(\alpha_{d,K})\rangle$, $\overline{\langle \tilde{\boldsymbol{W}}^{*}_{l,J}(\alpha_{d,J}),\ \boldsymbol{D}_{l,\ J\to K}\tilde{\boldsymbol{W}}_{l,K}(\alpha_{d,K})\rangle}$ is

$$\begin{aligned}&\overline{\langle \tilde{\boldsymbol{W}}^{*}_{l,J}(\alpha_{d,J}),\ \boldsymbol{D}_{l,\ J\to K}\tilde{\boldsymbol{W}}_{l,K}(\alpha_{d,K})\rangle}\\ &\quad=\int_{\alpha_{J,K},\beta_{J,K},\gamma_{J,K}}\langle \tilde{\boldsymbol{W}}^{*}_{l,J}(\alpha_{d,J}),\ \boldsymbol{D}_{l,\ J\to K}\tilde{\boldsymbol{W}}^{*}_{l,J}(\alpha_{d,J})\rangle\\ &\qquad\times C(\alpha_{J,K},\beta_{J,K},\gamma_{J,K})d\alpha_{J,K}\sin\beta_{J,K}d\beta_{J,K}d\gamma_{J,K}. \end{aligned}\quad (23)$$

$C(\alpha_{J,K},\beta_{J,K},\gamma_{J,K})$ is the PDF of domain J relative to domain K; hence,

$$\begin{aligned}&\int_{\alpha_{J,K},\beta_{J,K},\gamma_{J,K}}C(\alpha_{J,K},\beta_{J,K},\gamma_{J,K})d\alpha_{J,K}\sin\beta_{J,K}d\beta_{J,K}d\gamma_{J,K}\\ &\quad=1. \end{aligned}\quad (24)$$

Performing the integrations for orders $l\geqslant 1$ in Eq. (20), we obtain the following:

$$\begin{aligned}&\overline{\langle \tilde{\boldsymbol{W}}^{*}_{l,J}(\alpha_{d,J}),\ \boldsymbol{D}_{l,\ J\to K}\tilde{\boldsymbol{W}}_{l,K}(\alpha_{d,K})\rangle}\\ &\quad=\langle \tilde{\boldsymbol{W}}^{*}_{l,J}(\alpha_{d,J}),\boldsymbol{C}_{l,\ JK}(\alpha_{d,J},\alpha_{d,K})\tilde{\boldsymbol{W}}_{l,K}(\alpha_{d,K})\rangle, \end{aligned}\quad (25)$$

where $\boldsymbol{C}_{l;J,K}(\alpha_{d,J},\alpha_{d,K})$ is the matrix element $\frac{8\pi^2}{2l+1}C^{*\ m,m'}_{l}(\alpha_{d,J},\alpha_{d,K})$ [23]. This matrix depends on the types (e.g., circular, protruding, etc.) of interacting domains, and on their respective sizes.

2. Domains with circular symmetry

The results described thus far pertain to domains having the same size and shape (i.e., monodisperse). As described in a previous work [22], the Wigner functions can be reduced to Legendre polynomials, and only the terms containing $m=0,m'=0$ are involved; i.e.,

$$\begin{aligned}I(q)&=4\pi\left[2\sqrt{\pi}M_0(q)+\sum_J\tilde{W}_{0,J}(\alpha_{d,J};q)\right]^2\\ &\quad+4\pi\sum_J\sum_{l=1}^{\infty}|\tilde{W}_{l,J}(\alpha_{d,J};q)|^2\\ &\quad+4\pi\sum_{J\neq K}\sum_{l=1}^{\infty}\tilde{W}^{\,0}_{l,J}(\alpha_{d,J};q)\tilde{W}^{0}_{l,K}(\alpha_{d,K};q)P_l(\cos\theta_{JK}), \end{aligned}\quad (26)$$

where J and K represent domains, θ_{JK} is the angle between vectors pointing from the origin to domain centers J and K, and $\tilde{W}^{\,0}_{l,J}(\alpha_d;q)$ and $\tilde{W}^{0}_{l,K}(\alpha_d;q)$ (both real) are given by Eq. (18).

The PDF for domain centers depends only on the angle subtended by the chord between the two domain centers θ_{JK}. In this case, the generalized spherical functions are Legendre polynomials and the series expansions are carried out as in [22]. As a result, Eq. (25) simplifies to

$$\begin{aligned}&\overline{\langle \tilde{\boldsymbol{W}}^{*}_{l,J}(\alpha_{d,J}),\ \boldsymbol{D}_{l,\ J\to K}\tilde{\boldsymbol{W}}_{l,K}(\alpha_{d,K})\rangle}\\ &\quad=\tilde{W}^{\,0}_{l,J}(\alpha_{d,J};q)\tilde{W}^{0}_{l,K}(\alpha_{d,K};q)C_{l,\ JK}(\alpha_{d,J},\alpha_{d,K}). \end{aligned}\quad (27)$$

That is, the right-hand side of the equation contains a simple product instead of a bilinear form.

Variable thickness spanning domains. We recall that the term "domain" denotes an inclusion (e.g., lipid, protein, etc.) in the vesicle of different scattering "contrast"—e.g., due to a difference in chemical composition or isotopic content (see Fig. 1). Starting from the general form of $\omega(\boldsymbol{r})$ given in Methods, or

$$\omega(\boldsymbol{r})=\begin{cases}\rho_d(r,\theta,\varphi)-\rho_c(r), & (\theta,\varphi)_{\text{in}}\\ 0, & (\theta,\varphi)_{\text{out}}\end{cases}, \quad (28)$$

we introduce a simplified model, where for all domains it is assumed that the domain angle α_d varies along the thickness of the domain (R_o-R_i) as follows: $\omega(\boldsymbol{r})=\omega(r)\tilde{\omega}(\hat{r},r)$,

where

$$\omega(r) = \begin{cases} 0, & r < R_i \\ \rho_d(r) - \rho_c(r), & R_i \leqslant r \leqslant R_o, \\ 0, & r > R_o \end{cases} \tag{29}$$

$$\tilde{\omega}(\hat{r},r) = \tilde{\omega}(\theta,\varphi,r) = \begin{cases} 1, & 0 \leqslant \theta \leqslant \alpha_d(r) \\ 0, & \alpha_d(r) < \theta < \pi \end{cases}, \tag{30}$$

where R_i is the distance between the center of a spherical vesicle and the inner edge of the inner leaflet, R_o is the distance between the center of a vesicle and the outer edge of the outer leaflet (see Fig. 1), and α_d is the angular size of the domain (see Methods). It is important to note that these functions may also vary from domain to domain. This implies that the thickness of the spanning domain can vary as $R_i \leqslant r \leqslant R_o$, where the maximum value of the fully spanning domain is equal to the membrane thickness. In this case, Eq. (18) reduces to

$$\tilde{W}_l(q) = \int_0^\infty \omega(r) r^2 j_0(qr) \left(\int_0^{\alpha_d(r)} Y_l^{0*}(\hat{r}) d\hat{r} \right) dr. \tag{31}$$

Integrating over $\hat{r}$, i.e., (θ,φ), one obtains

$$\tilde{W}_l(q) = \int_0^\infty \omega(r) r^2 j_0(qr) \tilde{w}_l^0(\alpha_d(r)) dr. \tag{32}$$

An expression similar to that in [22] is given as

$$\begin{aligned} \tilde{w}_0(\alpha_d) &= \int_0^{2\pi} d\varphi \int_0^{\alpha_d(r)} Y_0^{0*}(\theta,\varphi) \sin\theta \, d\theta \\ &= \sqrt{\pi}(1 - \cos\alpha_d(r)), \end{aligned} \tag{33}$$

$$\begin{aligned} \tilde{w}_l^0(\alpha_d) = \frac{\sqrt{\pi(2l+1)}}{l} &[\cos\alpha_d(r) P_l(\cos\alpha_d) \\ &- P_{l+1}(\cos\alpha_d(r))]. \end{aligned} \tag{34}$$

The scattering cross sections can thus be written as

$$\begin{aligned} I(q) = 4\pi &\left[2\sqrt{\pi} M_0(q) + \sum_J \tilde{W}_{0,J}^0(q) \right]^2 \\ &+ 4\pi \sum_J \sum_{l=1}^\infty \left| \tilde{W}_{l,J}^0(q) \right|^2 \\ &+ 4\pi \sum_{J \neq K} \sum_{l=1}^\infty \tilde{W}_{l,J}^{0*}(q) \tilde{W}_{l,K}^0(q) P_l(\cos\theta_{JK}). \end{aligned} \tag{35}$$

If the domains are assumed to interact via a hard-core potential, the average of $P_l(\cos\theta_{JK})$ can be expressed as

$$\begin{aligned} \overline{I(q)} = 4\pi &\left[2\sqrt{\pi} M_0(q) + \sum_J \tilde{W}_{0,J}^0(q) \right]^2 \\ &+ 4\pi \sum_J \sum_{l=1}^\infty \left| \tilde{W}_{l,J}^0(q) \right|^2 \\ &+ 4\pi \sum_{J \neq K} \sum_{l=1}^\infty \tilde{W}_{l,J}^{0*}(q) \tilde{W}_{l,K}^0(q) C_l(\cos\theta_{JK;\min}). \end{aligned} \tag{36}$$

In the case where all domains are identical, $\cos\theta_{JK;\min} = 2\alpha_d$ is the minimum angle subtended on the vesicle surface by the domain centers. This is given in terms of α_d, the maximum value over all angles in $\boldsymbol{\alpha}_d$, as

$$\begin{aligned} I(q) = 4\pi &\left[2\sqrt{\pi} M_0(q) + N_d \tilde{W}_0^0(q) \right]^2 + 4\pi N_d \sum_{l=1}^\infty \left| \tilde{W}_l^0(q) \right|^2 \\ &+ 4\pi N_d (N_d - 1) \sum_{l=1}^\infty \left| \tilde{W}_l^0(q) \right|^2 C_l(2\alpha_d). \end{aligned} \tag{37}$$

For multilamellar vesicles, $M_0(q)$ is expressed in the manner (see Methods)

$$M_0(q) = \int_0^\infty \mu(r) r^2 j_0(qr) dr, \tag{38}$$

where $\mu(r)$ varies with r. This model includes several submodels, but we will discuss only two, namely, those of half and fully protruding domains.

Half protruding domains. Figure 1(b) shows a lipid bilayer with a protein extending beyond the vesicle surface. As was described in Methods, we can represent the case of a half protruding domain as

$$W_l(q, R_i, R_{i,\text{domain}}) = \frac{(\rho_d - \rho_m)}{q^3} \int_{qR_{i,\text{ domain}}}^{qR_i} z^2 j_l(z) dz, \tag{39}$$

where the inner radius of the vesicle is replaced by the inner radius of the domain [see Fig. 1(b)], $\tilde{W}_{l,J}^{0*}(q) = \tilde{w}_{l,J}^{0*} W_l(q, R_i, R_{i,\text{domain}})$, where $R_{i,\text{domain}}$ and $R_{o,\text{domain}}$ define the inner and outer protruding parts of the domain. In the case where a vesicle contains a domain spanning the vesicle thickness, Eq. (39) is modified to yield

$$\begin{aligned} W_l(q, R_i, R_i, R_{o,\text{domain}}) = &\frac{(\rho_d - \rho_m)}{q^3} \int_{qR_{i,\text{domain}}}^{qR_{i,}} z^2 j_l(z) dz \\ &+ \frac{(\rho_d - \rho_c)}{q^3} \int_{qR_i}^{qR_{o,\text{domain}}} z^2 j_l(z) dz. \end{aligned} \tag{40}$$

In this case, all domains have the same radii (i.e., they are monodisperse), and the factors $\tilde{w}_l^0(\alpha_d)$ are unaffected.

Fully protruding domains. The more complicated case of a protruding domain is solved in two parts. First, we modified the circular domain scenario presented in [22] to apply to a protruding domain, as explained in Appendix B in [24]. The only difference is $\tilde{w}_l^0(\alpha_d)$, namely,

$$\begin{aligned} \tilde{w}_0(\alpha_{\text{in}}, \alpha_d) &= \int_0^{2\pi} d\varphi \int_{\alpha_{\text{in}}}^{\alpha_d} Y_0^{0*}(\theta,\varphi) \sin\theta \, d\theta \\ &= \sqrt{\pi}(\cos\alpha_{\text{in}} - \cos\alpha_d). \end{aligned} \tag{41}$$

Hence,

$$\begin{aligned} \tilde{w}_l^0(\alpha_{\text{in}}, \alpha_d) &= 2\pi \int_{\alpha_{\text{in}}}^{\alpha_d} \left(\frac{2l+1}{4\pi} \right)^{1/2} P_l(\cos\theta) \sin\theta d\theta \\ &= \sqrt{\pi(2l+1)} \int_{\cos\alpha_d}^{\cos\alpha_{\text{in}}} P_l(x) dx \end{aligned} \tag{42}$$

and

$$\tilde{w}_l^0(\cos\alpha_{\rm in},\alpha_d) = \frac{\sqrt{\pi(2l+1)}}{l}[\cos\alpha_d P_l(\cos\alpha_d) - P_{l+1}(\cos\alpha_d) - \cos\alpha_{\rm in} P_l(\cos\alpha_{\rm in}) + P_{l+1}(\cos\alpha_{\rm in})], \quad (43)$$

where $\alpha_{\rm in}$ is the angular size of the domain, and $\alpha_{\rm in} < \alpha_d$. Note that the interdomain correlation functions remain unaltered because the domains are hard. In other words, for a fully protruding domain with circular symmetry the remaining equations are identical to those for a spanning domain with circular symmetry. The angular part, $\tilde{w}_l^0(\cos\alpha_{\rm in},\alpha_d)$, remains constant through the length of the domain; however, the radial component includes the following three terms describing (i) the protruding domain portion inside the vesicle, (ii) the domain part spanning the thickness of the vesicle, and (iii) the protruding domain portion extending beyond the vesicle. These terms are related as follows:

$$W_l(q,R_i,R_o,R_{i,\rm domain},R_{o,\rm domain}) = \frac{(\rho_d-\rho_m)}{q^3}\int_{qR_{i,\rm domain}}^{qR_{i,}} z^2 j_l(z)dz + \frac{(\rho_d-\rho_c)}{q^3}\int_{qR_i}^{qR_o} z^2 j_l(z)dz + \frac{(\rho_d-\rho_m)}{q^3}\int_{qR_o}^{qR_{o,\rm domain}} z^2 j_l(z)dz. \quad (44)$$

The fully protruding domain allows the model more flexibility; i.e., a domain with protrusions inside and outside a vesicle can be modeled as a combination of spanning and half protruding domains, as shown in Figs. 1(a) and 1(b). Therefore, as in the case of the spanning domains with circular symmetry, we can describe such a scenario as

$$\tilde{W}_l(q,R_i,R_m,R_o) = \sum_{K=1}^{N}\tilde{w}_l^0(\alpha_{i,K},\alpha_{o,K})W_l(q,R_{i,K},R_{o,K}), \quad (45)$$

where $\alpha_{i,K}=0$. The maximum angle used to characterize the correlation between domain centers is given by

$$\max_{1\leqslant K\leqslant N}\alpha_{o,K}. \quad (46)$$

B. Probability distribution between centers of domain pairs

1. The case of two spanning domains with circular symmetry

To begin with, we assume that domain centers are uniformly distributed in their allowed region and that the domains are hard, implying that they interact via a hard-core potential. As a result, we obtain the following PDF:

$$C(\alpha,\cos\theta_{JK},\gamma) = \begin{cases} 0, & 1 \geqslant \cos\theta_{JK} \geqslant \cos(\alpha_{d,J}+\alpha_{d,K}) \\ S, & \cos(\alpha_{d,J}+\alpha_{d,K}) > \cos\theta_{JK} < -1 \end{cases}. \quad (47)$$

To simplify the notation, we denote

$$\theta_{JK;\rm min} = \alpha_{d,J}+\alpha_{d,K}. \quad (48)$$

The constant S in Eq. (47) is determined by denoting it as a PDF $C(\alpha,\beta,\gamma)$ satisfying Eq. (24):

$$4\pi^2 S(1+\cos\theta_{JK;\rm min}) = 1. \quad (49)$$

Hence, the average is

$$\overline{P_l(\cos\theta_{JK})} = 4\pi^2 S\int_{-1}^{\cos\theta_{JK;\rm min}} P_l(x)dx = \frac{[(P_{l+1}(x)-xP_l(x))]|_{-1}^{\cos\theta_{JK;\rm min}}}{l(1+\cos\theta_{JK;\rm min})} = C_l(\theta_{JK;\rm min}). \quad (50)$$

One has also to consider that

$$\int_{-1}^{1} P_l(x)dx, \quad l>0. \quad (51)$$

This leads to

$$\int_{-1}^{\cos\theta_{JK;\rm min}} P_l(x)dx = -\int_{\cos\theta_{JK;\rm min}}^{1} P_l(x)dx, \quad (52)$$

and

$$\overline{P_l(\cos\theta_{JK})} = -\frac{[(P_{l+1}(x)-xP_l(x))]|_{\cos\theta_{JK;\rm min}}^{1}}{l(1+\cos\theta_{JK;\rm min})} = C_l(\theta_{JK;\rm min}). \quad (53)$$

Thus, the average over different domains with circular symmetry on a vesicle's surface is given by

$$\overline{I(q)} = 4\pi\left[2\sqrt{\pi}M_0(q)+\sum_J \tilde{w}_{0,J}(\alpha_{d,J})W_{0,J}(q)\right]^2 + 4\pi\sum_J\sum_{l=1}^{\infty}\left|\tilde{w}_{l,J}^0(\alpha_d)W_{l,J}(q)\right|^2 + 4\pi\sum_{J\neq K}\sum_{l=1}^{\infty}\tilde{w}_{l,J}^0(\alpha_d)W_{l,J}^*(q)\tilde{w}_{l,K}^0(\alpha_d)W_{l,K}(q) \times C_l(\cos\theta_{JK;\rm min}). \quad (54)$$

In the case of identical size domains this yields

$$I(q) = 4\pi[2\sqrt{\pi}M_0(q)+N_d\tilde{w}_0(\alpha_d)W_0(q)]^2 + 4\pi N_d\sum_{l=1}^{\infty}\left|\tilde{w}_l^0(\alpha_d)\right|^2|W_l(q)|^2 + 4\pi N_d(N_d-1)\sum_{l=1}^{\infty}\left|\tilde{w}_l^0(\alpha_d)\right|^2|W_l(q)|^2C_l(2\alpha_d). \quad (55)$$

This model is exact for the case of two domains. Moreover, the model is also expected to be valid when the total surface of these domains is small compared to the vesicle total surface area.

2. The case of two or more identical spanning domains

A general solution for two or more domains. Analysis for the two-domain correlation function is similar to correlation functions in Euclidean space. In other words, it involves distances and an integral over the volume in Euclidean n-dimensional space. The volume element in Euclidean space corresponds to the unit sphere surface integral over $d\vec{\Omega}=\sin\theta d\theta d\varphi$, while the lengths correspond to the minimum arclength (geodesic) between two points having directions $\vec{\Omega}$ and $\vec{\Omega}'$. The minimum

arclength between these points is given by the arccos $(\vec{\Omega}\cdot\vec{\Omega}')$; for convenience, the functions are assumed to depend on the scalar product $\vec{\Omega}\cdot\vec{\Omega}'$, as it is easier to analyze this in spherical coordinates. Isotropy of the potential translates to a dependence of the potential only for the smallest arclength between two domain centers. As was pointed out earlier, the domains interact only through a hard-core potential.

We define the PDF as

$$H(\alpha_1,\alpha_2,\vec{\Omega}_1\cdot\vec{\Omega}_2)=\exp(-V_{1,2}(\vec{\Omega}_1\cdot\vec{\Omega}_2)), \tag{56}$$

where $V_{1,2}(\vec{\Omega}_1\cdot\vec{\Omega}_2)$ is the potential for two domains located at $\vec{\Omega}_1$ and $\vec{\Omega}_2$, and is defined as

$$H(\alpha_1,\alpha_2,\vec{\Omega}_1\cdot\vec{\Omega}_2)=\begin{cases}0, & 1\geqslant\vec{\Omega}_1\cdot\vec{\Omega}_2\geqslant\cos(\alpha_1+\alpha_2)\\ 1, & \cos(\alpha\,)>\vec{\Omega}_1\cdot\vec{\Omega}_2<-1\end{cases}. \tag{57}$$

Similar to the Euclidean space correlation function (see [25]), for the case of more than two domains, we define

$$C_{\rm full}(\vec{\Omega}_1\cdot\vec{\Omega}_2)=\frac{\iiint_{3,\,4,\ldots,N}\prod_{i=3}^{n}d\vec{\Omega}_{\rm i}\prod_{1<i<j<N}\exp(-V_{i,j}(\vec{\Omega}_{\rm i}\cdot\vec{\Omega}_{\rm j}))}{\iiint_{2,\ldots N}\prod_{i=2}^{n}d\vec{\Omega}_{\rm i}\prod_{1<i<j<N}\exp(-V_{i,j}(\vec{\Omega}_{\rm i}\cdot\vec{\Omega}_{\rm j}))}. \tag{58}$$

Equation (58) can be rewritten as

$$C_{\rm full}(\alpha_1,..,\alpha_N,\vec{\Omega}_1\cdot\vec{\Omega}_2)=\frac{\iiint_{3,\,4,\ldots,N}\prod_{i=3}^{n}d\vec{\Omega}_{\rm i}\prod_{1<i<j<N}{\rm H}(\alpha_i,\alpha_j,\vec{\Omega}_{\rm i}\cdot\vec{\Omega}_{\rm j})}{\iiint_{2,\ldots,N}\prod_{i=2}^{n}d\vec{\Omega}_{\rm i}\prod_{1<i<j<N}{\rm H}(\alpha_i,\alpha_j,\vec{\Omega}_{\rm i}\cdot\vec{\Omega}_{\rm j})}. \tag{59}$$

An important difference between Euclidean space and a spherical surface is that, because a sphere is bounded, the number of domains on a spherical surface is finite. However, if there are processes that add or remove domains from the spherical surface, one can then introduce a chemical potential, a notion that will not be developed any further in this paper.

The case of three domains. For any approximate equation it is useful to have examples where the exact solution is known. For the case of spanning domains on a spherical surface, the case of three domains allows for such a solution. This solution can then be used as a model for any approximation of domain distribution, because the number of domains is small, and their areas can be varied.

For the three-domain case we assume that the first domain is located at the sphere's north pole, and the positions of the second and third domains are defined by the angles θ_2, φ_2 and θ_3, φ_3, respectively, or as

$$C_{\rm full}(\alpha_1,\alpha_2,\alpha_3,\vec{\Omega}_1\cdot\vec{\Omega}_2)=\frac{{\rm H}(\alpha_1,\alpha_2,\,\vec{\Omega}_1\cdot\vec{\Omega}_2)\iiint d\vec{\Omega}_3{\rm H}(\alpha_2,\alpha_3,\,\vec{\Omega}_2\cdot\vec{\Omega}_3){\rm H}(\alpha_1,\alpha_3,\,\vec{\Omega}_1\cdot\vec{\Omega}_3)}{\iiint d\vec{\Omega}_2d\vec{\Omega}_3{\rm H}(\alpha_1,\alpha_2,\,\vec{\Omega}_1\cdot\vec{\Omega}_2){\rm H}(\alpha_2,\alpha_3,\,\vec{\Omega}_2\cdot\vec{\Omega}_3){\rm H}(\alpha_1,\alpha_3,\,\vec{\Omega}_1\cdot\vec{\Omega}_3)}. \tag{60}$$

Since the numerator is a constant, only the integral of the numerator needs to be evaluated. However, having a geometric interpretation helps us to evaluate the integral. The two H functions denote the joint exclusion areas around the two domains, and the integral estimates the area into which the center of the third domain is allowed. Its complement is called the exclusion area. When far from each other, the exclusion areas are not in contact. The total area permitted for the third domain center is thus any area that is not occupied by the two exclusion zones, i.e.,

$$4\pi-2\pi(1-\cos(\alpha_2+\alpha_3))-2\pi(1-\cos(\alpha_1+\alpha_3)). \tag{61}$$

However, when the domains approach each other, at first, their exclusion areas become tangential, and then they intersect. Hence, the total exclusion area is smaller than the sum of the exclusion areas, as shown in Fig. 2.

We denote the angle of separation between the two domain centers as β. To compute the total exclusion area, one has to estimate the areas of the two domain sectors and of the two congruent "spherical" triangles whose sides are related by angles $\alpha_2+\alpha_3$, $\alpha_1+\alpha_3$, and β. The area of one triangle is

$$s_\Delta=A+B+C-\pi, \tag{62}$$

and the domain sectors have areas

$$\begin{aligned}s_1&=(2\pi-2C)(1-\cos(\alpha_2+\alpha_3)),\\ s_2&=(2\pi-2A)(1-\cos(\alpha_1+\alpha_3)),\end{aligned} \tag{63}$$

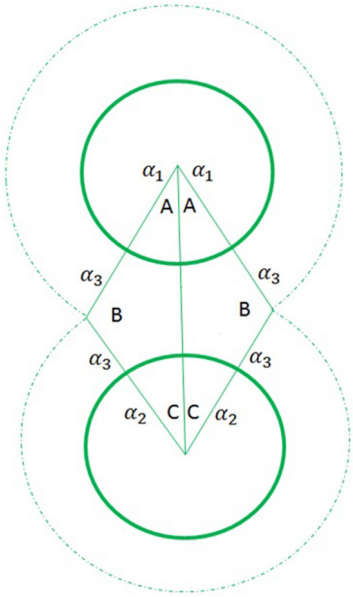

FIG. 2. Spherical geometry of two domains (circles) and their exclusion zones. The domain boundaries are depicted by the thick lines. The exclusion area boundaries are shown by the dashed curves. To highlight the difference between the domains and the triangle on the sphere ("spherical" triangle), the triangle's sides are drawn as straight lines.

where

$$\cos A = \frac{\cos(\alpha_2+\alpha_3) - \cos\beta\cos(\alpha_2+\alpha_3)}{\sin\beta\sin(\alpha_2+\alpha_3)}, \tag{64}$$

$$\cos B = \frac{\cos\beta - \cos(\alpha_2+\alpha_3)\cos(\alpha_2+\alpha_3)}{\sin(\alpha_2+\alpha_3)\mathrm{sins}(\alpha_2+\alpha_3)}, \tag{65}$$

$$\cos C = \frac{\cos(\alpha_1+\alpha_3) - \cos\beta\cos(\alpha_1+\alpha_3)}{\sin\beta\sin(\alpha_1+\alpha_3)}. \tag{66}$$

Equations (48) and (49) are the equations for "spherical" triangles in a spherical geometry [26]. β varies between $\alpha_1+\alpha_2$ and $\alpha_1+\alpha_2+2\alpha_3$ so that the domains do not touch each other, but their exclusion areas still intersect. The free area is then given by

$$\iiint_3 d\vec{\Omega}_3 \mathrm{H}(\alpha, \vec{\Omega}_2\cdot\vec{\Omega}_3)\mathrm{H}(\alpha, \vec{\Omega}_1\cdot\vec{\Omega}_3) = \begin{cases} 4\pi - 2\pi(1-\cos(\alpha_2+\alpha_3)) - 2\pi(1-\cos(\alpha_1+\alpha_3)) & \text{if } \beta > \alpha_1+\alpha_2+2\alpha_3 \\ 4\pi - s_1 - s_2 - 2s_\Delta & \text{if } \alpha_1+\alpha_2 \leqslant \beta \leqslant \alpha_1+\alpha_2+2\alpha_3. \end{cases} \tag{67}$$

To normalize this function, the nominator can be obtained by numerical integration of the numerator. Also, the computation of the Legendre coefficients of the normalized correlation function is best performed by numerical quadrature. It is important to mention that the exact solution for the case of more than three domains is nontrivial.

C. Positionally correlated and uncorrelated domains

Here, we describe cases where the inner leaflet domain is positionally correlated across the membrane with an outer leaflet domain, and where the two domains can move independently of each other (i.e., not positionally correlated to each other). In both cases, we looked at deterministic and random distributions of domains on a vesicle.

In the case where domains are positionally correlated, the domains can be described as having angles $\alpha_{d,\mathrm{in}}$ and $\alpha_{d,\mathrm{out}}$, and densities $\rho_{d,\mathrm{in}}$ and $\rho_{d,\mathrm{out}}$. The lipid bilayer has densities $\rho_{c,\mathrm{in}}$ and $\rho_{c,\mathrm{out}}$, and the interface between the inner and outer leaflets (see Fig. 1) is of radius R_m.

$\tilde{W}_l$ can thus be written as

$$\begin{aligned}\tilde{W}_l(q,R_i,R_m,R_o) &= \tilde{w}_l^0(\alpha_{d,\mathrm{in}})\frac{(\rho_{d,\mathrm{in}}-\rho_{c,\mathrm{in}})}{q^3}\int_{qR_i}^{qR_m} z^2 j_l(z)dz \\ &+ \tilde{w}_l^0(\alpha_{d,\mathrm{out}})\frac{(\rho_{d,\mathrm{out}}-\rho_{c,\mathrm{out}})}{q^3}\int_{qR_m}^{qR_o} z^2 j_l(z)dz,\end{aligned} \tag{68}$$

or as

$$\begin{aligned}\tilde{W}_l(q,R_i,R_m,R_o) &= \tilde{w}_l^0(\alpha_{d,\mathrm{in}})W_l(q,R_i,R_m) \\ &+ \tilde{w}_l^0(\alpha_{d,\mathrm{out}})W_l(q,R_m,R_o).\end{aligned} \tag{69}$$

This equation is useful when the difference between the two cases of domains (positionally correlated or uncorrelated) needs to be computed. If one assumes that the domains are positioned at fixed angles θ_{JK} to each other, and the inner and outer leaflet domains are positionally correlated, the scattered intensity can be written as follows:

$$\begin{aligned}I_1(q) = 4\pi&\left[2\sqrt{\pi}M_0(q) + \sum_J\left[\tilde{w}_{0,J}^0(\alpha_{d,\mathrm{in}})W_0(q,R_i,R_m) + \tilde{w}_{0,J}^0(\alpha_{d,\mathrm{out}})W_0(q,R_m,R_o)\right]\right]^2 \\ &+ 4\pi\sum_J\sum_{l=1}^{\infty}\left|\tilde{w}_l^0(\alpha_{d,\mathrm{in}})W_l(q,R_i,R_m) + \tilde{w}_l^0(\alpha_{d,\mathrm{out}})W_l(q,R_m,R_o)\right|^2 \\ &+ 4\pi\sum_{J\neq K}\sum_{l=1}^{\infty}\left[\tilde{w}_{0,J}^{0*}(\alpha_{d,\mathrm{in}})W_0(q,R_i,R_m) + \tilde{w}_{0,J}^{0*}(\alpha_{d,\mathrm{out}})W_0(q,R_m,R_o)\right] \\ &\times\left[\tilde{w}_{0,J}^0(\alpha_{d,\mathrm{in}})W_0(q,R_i,R_m) + \tilde{w}_{0,J}^0(\alpha_{d,\mathrm{out}})W_0(q,R_m,R_o)\right]P_l(\cos\theta_{JK}).\end{aligned} \tag{70}$$

However, when the inner and outer leaflet domains are positionally independent of each other, the scattered intensity is

$$\begin{aligned}I_2(q) = 4\pi&\left[2\sqrt{\pi}M_0(q) + \sum_J\tilde{w}_{0,J}^0(\alpha_{d,\mathrm{in}})W_0(q,R_i,R_m) + \sum_J\tilde{w}_{0,J}^0(\alpha_{d,\mathrm{out}})W_0(q,R_m,R_o)\right]^2 \\ &+ 4\pi\sum_J\sum_{l=1}^{\infty}\left|\tilde{w}_{l,J}^0(\alpha_{d,\mathrm{in}})W_l(q,R_i,R_m)\right|^2 + 4\pi\sum_J\sum_{l=1}^{\infty}\left|\tilde{w}_{l,J}^0(\alpha_{d,\mathrm{out}})W_l(q,R_m,R_o)\right|^2\end{aligned}$$

$$+4\pi\sum_{J\neq K}\sum_{l=1}^{\infty}\mathrm{Re}\left[\tilde{w}^{0*}_{l,J}(\alpha_{d,\mathrm{in}})W_l(q,R_i,R_m)\tilde{w}^{0}_{l,K}(\alpha_{d,\mathrm{in}})W_l(q,R_i,R_m)\right]P_l(\cos\theta_{JK})$$

$$+4\pi\sum_{J\neq K}\sum_{l=1}^{\infty}\mathrm{Re}\left[\tilde{w}^{0*}_{l,J}(\alpha_{d,\mathrm{out}})W_l(q,R_m,R_o)\tilde{w}^{0}_{l,K}(\alpha_{d,\mathrm{out}})W_l(q,R_m,R_o)\right]P_l(\cos\theta_{JK}), \tag{71}$$

where Re is the real part of a complex number.

The difference between positionally correlated and uncorrelated N identical domains of each type can be expressed as

$$I_1(q)-I_2(q)=8\pi N\sum_{l=1}^{\infty}\mathrm{Re}\left[\tilde{w}^{0*}_{l}(\alpha_{d,\mathrm{in}})W_l(q,R_i,R_m)\tilde{w}^{0}_{l}(\alpha_{d,\mathrm{out}})W_l(q,R_m,R_o)\right]$$

$$+8\pi\sum_{J\neq K}\sum_{l=1}^{\infty}\mathrm{Re}\left[\tilde{w}^{0*}_{l,J}(\alpha_{d,\mathrm{in}})W_l(q,R_i,R_m)\tilde{w}^{0}_{l,K}(\alpha_{d,\mathrm{out}})W_l(q,R_m,R_o)\right]P_l(\cos\theta_{JK}). \tag{72}$$

In this case, the only terms that differ are the ones containing averages over $P_l(\cos\theta_{JK})$.

If, however, the domains repel each other, their distribution will be fixed. For instance, four domains will arrange themselves at the vertices of a tetrahedron, while eight domains occupy the vertices of a cube. If the number of domains does not equal the vertices of a regular polyhedral, they will arrange themselves in the most regular manner possible. If, however, the domains do not interact with each other—except through rigid body forces—then the quantity of interest is the site-site correlation function averaged over all possible domain arrangements on a spherical vesicle. This is given by

$$4\pi N(N-1)\sum_{l=1}^{\infty}\left|\tilde{w}^{0*}_{l}(\alpha_{d,\mathrm{in}})W_l(q,R_i,R_m)+\tilde{w}^{0*}_{l}(\alpha_{d,\mathrm{out}})W_0(q,R_m,R_o)\right|^2 C_l(2\max(\alpha_{d,\mathrm{in}},\alpha_{d,\mathrm{out}})), \tag{73}$$

while in the case of domains with fixed positions the relationship is written as

$$4\pi N(N-1)\left[\sum_{l=1}^{\infty}\left|\tilde{w}^{0*}_{l}(\alpha_{d,\mathrm{in}})W_l(q,R_i,R_m)\right|^2 C_l(2\alpha_{d,\mathrm{in}})+\sum_{l=1}^{\infty}\left|\tilde{w}^{0*}_{l}(\alpha_{d,\mathrm{out}})W_0(q,R_m,R_o)\right|^2 C_l(2\alpha_{d,\mathrm{out}})\right]. \tag{74}$$

The difference between the two terms is given by

$$\bar{I}_1(q)-\bar{I}_2(q)=8\pi N\sum_{l=1}^{\infty}\mathrm{Re}\left[\tilde{w}^{0*}_{l}(\alpha_{d,\mathrm{in}})W_l(q,R_i,R_m)\tilde{w}^{0}_{l}(\alpha_{d,\mathrm{out}})W_l(q,R_m,R_o)\right]$$

$$+4\pi N(-1)\Bigg[2\sum_{l=1}^{\infty}\mathrm{Re}\left[\tilde{w}^{0*}_{l}(\alpha_{d,\mathrm{in}})W_l(q,R_i,R_m)\tilde{w}^{0*}_{l}(\alpha_{d,\mathrm{out}})W_0(q,R_m,R_o)\right]C_l(2\max(\alpha_{d,\mathrm{in}},\alpha_{d,\mathrm{out}})$$

$$+\sum_{l=1}^{\infty}\left|\tilde{w}^{0*}_{l}(\alpha_{d,\mathrm{in}})W_l(q,R_i,R_m)\right|^2(C_l(2\max(\alpha_{d,\mathrm{in}},\alpha_{d,\mathrm{out}})-C_l(2\alpha_{d,\mathrm{in}}))$$

$$+\sum_{l=1}^{\infty}\left|\tilde{w}^{0*}_{l}(\alpha_{d,\mathrm{out}})W_0(q,R_m,R_o)\right|^2(C_l(2\max(\alpha_{d,\mathrm{in}},\alpha_{d,\mathrm{out}})-C_l(2\alpha_{d,\mathrm{out}}))\Bigg]. \tag{75}$$

For the case of more than three domains, a better option is to use an approximation of the PY equation (see [27]) adapted for a spherical surface. This scenario is described below.

D. Equations for domains on a spherical surface

Following the studies of rigid disks in the Euclidean plane [28,29], a PY type of approximation [30] is best suited in describing domains on a spherical surface. Solving the PY equation results in an approximate, but accurate, solution to the two-dimensional rigid disk problem in the Euclidean plane [28,29]. Therefore, by solving a "spherical" analog of the PY equation, one could calculate pair correlations between more than two spanning domains with circular symmetry. Although the topology of a spherical surface does not allow for an infinite distance between domains, it does allow for a form of isotropy and for a metric tensor. We begin with an analog of the OZ equation using the PY conditions.

E. The OZ equation for hard domains on a spherical surface

In obtaining the OZ equation for identical domains on a spherical surface we start from the general case, where the potential is short range: we adapted the methods from [27] and the solution found in [31] for a fixed number of hard spheres in a box of fixed volume.

An analog of the isotropy condition on a spherical surface is that the two-domain potential depends only on the length of the geodesic uniting the points i and j, i.e., the $\arccos(\vec{\Omega}_\mathrm{i}\cdot\vec{\Omega}_\mathrm{j})$, where Ω is the solid angle and $\vec{\Omega}$ is defined as $\vec{\Omega}=[\sin\theta\cos\varphi,\sin\theta\sin\varphi,\cos\theta]$. At a practical level,

a dependence on the scalar product $\vec{\Omega}_i \cdot \vec{\Omega}_j$ is preferable. The configurational integral is thus given by

$$Z_N = \iiint_{1,\ldots,N} \prod_{i=1}^{n} d\vec{\Omega}_i \prod_{i<j;i,j<N} \exp(-V(\vec{\Omega}_i \cdot \vec{\Omega}_j)). \tag{76}$$

As we develop the theory, differences between the spherical surface and Euclidean cases are presented for the spherical case. The "translational invariance" (that is, moving on a circle irrespective of distance) for the spherical case yields

$$P_N^{(1)}(\vec{\Omega}_1) = \frac{\iiint_{2,\ldots,N;\vec{\Omega}_1 \text{fixed}} \prod_{i=1}^{n} d\vec{\Omega}_i \prod_{i<j;i,j<N} \exp(-V(\vec{\Omega}_i \cdot \vec{\Omega}_j))}{\iiint_{1,\ldots,N} \prod_{i=1}^{n} d\vec{\Omega}_i \prod_{i<j;i,j<N} \exp(-V(\vec{\Omega}_i \cdot \vec{\Omega}_j))} = \frac{1}{4\pi}. \tag{77}$$

As in the case of Euclidean space, when the domains are small they are expected to move quasi-independently. One can therefore take the ratio of the multidomain probability and divide it by the respective single-domain probabilities as follows:

$$g_N^{(n)}(\vec{\Omega}_1, \ldots, \vec{\Omega}_n) = \frac{P_N^{(n)}(\vec{\Omega}_1, \ldots, \vec{\Omega}_n)}{\prod_{i=1}^{n} P_N^{(1)}(\vec{\Omega}_i)} = (4\pi)^n P_N^{(n)}(\vec{\Omega}_1, \ldots, \vec{\Omega}_n), \tag{78}$$

where $P_N^{(n)}(\vec{\Omega}_1, \ldots, \vec{\Omega}_n)$ is defined similarly to $P_N^{(1)}(\vec{\Omega}_1)$, but instead of just $\vec{\Omega}_1$ being removed from the integration in the numerator, all variables $\vec{\Omega}_1, \ldots, \vec{\Omega}_n$ are deleted. The function $C_{\text{full}}(\vec{\Omega}_1 \cdot \vec{\Omega}_2)$, used previously, is equal to

$$C_{\text{full}}(\vec{\Omega}_1 \cdot \vec{\Omega}_2) = \frac{P_N^{(2)}(\vec{\Omega}_1, \vec{\Omega}_2)}{P_N^{(1)}(\vec{\Omega}_1)} = g_N^{(2)}(\vec{\Omega}_1, \vec{\Omega}_2) P_N^{(1)}(\vec{\Omega}_1) = \frac{1}{4\pi} g_N^{(2)}(\vec{\Omega}_1, \vec{\Omega}_2). \tag{79}$$

Because $g_N^{(2)}(\vec{\Omega}_1, \vec{\Omega}_2)$ depends only on the minimum circle arclength joining points $\vec{\Omega}_1$ and $\vec{\Omega}_2$, $g_N^{(2)}(\vec{\Omega}_1, \vec{\Omega}_2) = g_N^{(2)}(\vec{\Omega}_1 \cdot \vec{\Omega}_2)$. The function $g_N^{(2)}(\vec{\Omega}_1 \cdot \vec{\Omega}_2)$ is the spherical surface analog of the radial distribution function and is specific to the spherical case. As only $g_N^{(2)}$ was used, $g_N^{(2)} = g_N$.

Since a spherical surface is closed, the domains cannot escape it by moving. If the number of domains, N, is constant, an approximate OZ equation can be developed, as was done in [31]. It should be pointed out that proofs (not shown) for the N finite case are similar to those in [31], except for changes to the appropriate volume elements and geodesic length (arclength) for distance.

To obtain an OZ type of equation when N is fixed, we follow the procedure outlined in [31], while making appropriate modifications to account for the spherical surface case. This is written as follows:

$$\int_S \rho_N(\vec{\Omega}) d\vec{\Omega} = N, \tag{80}$$

$$\int_S \rho_N^2(\vec{\Omega}_1, \vec{\Omega}_2) d\vec{\Omega}_2 = (N-1)\rho_N(\vec{\Omega}_1), \tag{81}$$

$$\rho_N^2(\vec{\Omega}_1, \vec{\Omega}_2) = \rho_N(\vec{\Omega}_1)\rho_N(\vec{\Omega}_2) g_N(\vec{\Omega}_1, \vec{\Omega}_2), \tag{82}$$

$$\int_S \rho_N(\vec{\Omega}_1) g_N(\vec{\Omega}_1, \vec{\Omega}_2) d\vec{\Omega}_1 = (N-1). \tag{83}$$

Defining

$$h_N(\vec{\Omega}_1, \vec{\Omega}_2) = g_N(\vec{\Omega}_1, \vec{\Omega}_2) - 1 \tag{84}$$

implies

$$\int_S \rho_N(\vec{\Omega}_1) h_N(\vec{\Omega}_1, \vec{\Omega}_2) d\vec{\Omega}_1 = -1. \tag{85}$$

As in [20], one can introduce a potential. This potential for a finite N generates the variational functional

$$\mathcal{F} = \hat{F} + \lambda_N \int_S \rho_N(\vec{\Omega}) d\vec{\Omega} = F(\lambda_N, \rho_N) - \int_S \rho_N(\vec{\Omega}) V_{\text{ext}}(\vec{\Omega}, \lambda_N, [\rho_N]) d\vec{\Omega}. \tag{86}$$

The remaining variational calculus and algebra are similar to those in [31] and do not involve geometry. For the case where N is fixed [31], the corresponding OZ equation is written as

$$h_N(\cos\theta) - c_N(\cos\theta) - \rho \int c_N(\cos\theta') h_N(\overrightarrow{\Omega'} \cdot \vec{\Omega}) \sin\theta' d\theta' d\varphi' + \frac{1}{N} = 0 \tag{87}$$

and, as previously,

$$h_N(\cos\theta) = g_N(\cos\theta) - 1. \tag{88}$$

The PY conditions for the functions g_N and c_N on the spherical surface are given as

$$g(\cos\theta) = 0, \quad \cos\theta < \cos 2\alpha_d, \tag{89}$$

$$c(\cos\theta) = 0, \quad \cos\theta > \cos 2\alpha_d. \tag{90}$$

F. Expansion of PY into Legendre polynomials

The expansion of the PY equation in Legendre polynomials has the advantage that it yields, practically directly (up to the normalization), the interdomain coefficients. Using Legendre polynomials for finite N domains, the OZ equation on a spherical surface transforms into a form that is similar to the Fourier transform of the OZ equation in Euclidian space. The starting point is

$$g_N(\cos\theta) - 1 - c_N(\cos\theta) - \rho \int c_N(\cos\theta')(g_N(\overrightarrow{\Omega'} \cdot \vec{\Omega}) - 1) \sin\theta' d\theta' d\varphi' + \frac{1}{N} = 0. \tag{91}$$

Dropping the index N, the density term is given explicitly as

$$\rho = \frac{N}{4\pi}. \tag{92}$$

Equation (91) then becomes

$$g(\cos\theta) - 1 - c(\cos\theta) - \frac{N}{4\pi}\int c(\cos\theta')(g(\vec{\Omega}'\cdot\vec{\Omega}) - 1)\sin\theta' d\theta' d\varphi' + \frac{1}{N} = 0. \tag{93}$$

Following the strategy used to solve the PY equation in Fourier space [32], Eq. (93) can be written as

$$g(\cos\theta) - c(\cos\theta) = 1 - \frac{N}{4\pi}\int c(\cos\theta')(g(\vec{\Omega}'\cdot\vec{\Omega}) - 1) \times \sin\theta' d\theta' d\varphi' + \frac{1}{N}. \tag{94}$$

Since the right-hand side of the equation is a continuous function of $\cos\theta$, we can define the following continuous function:

$$\tau(\cos\theta) = g(\cos\theta) - c(\cos\theta). \tag{95}$$

Equation (91) can be rewritten as two equations involving $\tau(\cos\theta)$ and $g(\cos\theta)$, namely,

$$\tau(\cos\theta) = 1 + \frac{N}{4\pi}\int [\tau(\cos\theta') - g(\cos\theta')] \times (g(\vec{\Omega}'\cdot\vec{\Omega}) - 1)\sin\theta' d\theta' d\varphi' + \frac{1}{N}$$

and

$$g(\cos\theta) = \tau(\cos\theta)\kappa\left(-1, \cos 2\alpha_d; \cos\theta'\right), \tag{96}$$

where $\kappa(-1, \cos 2\alpha_d; \cos\theta')$ is equal to 1 for the interval $[-1, \cos 2\alpha_d]$, and is zero elsewhere.

To proceed further, one has to consider the Legendre coefficients $\hat{f}_l$ of a function $f(\cos\theta)$ as a form of the integral transform. These coefficients are given by

$$\hat{f}_l = \int_0^\pi f(\cos\theta) P_l(\cos\theta)\sin\theta d\theta. \tag{97}$$

As in the case of other transforms, a convolution operation is defined by the convolution of Legendre polynomials given by [33], which we adapted as

$$\hat{e}_l \hat{f}_l \leftrightarrow \frac{1}{2\pi}\int_S e(\cos\theta') f(\vec{\Omega}'\cdot\vec{\Omega}) d\vec{\Omega}' \tag{98}$$

with

$$\vec{\Omega} = [\sin\theta, 0, \cos\theta] \tag{99}$$

and where S is the unit sphere surface.

The equation for the zero-order coefficients is relatively involved, i.e.,

$$\hat{\tau}_0 - 2 - \frac{N}{2}\left(\hat{\tau}_0\hat{g}_0 - \hat{g}_0^2 - \hat{\tau}_0 + \hat{g}_0\right) + \frac{2}{N} = 0, \tag{100}$$

while those for the higher orders have a simpler form, i.e.,

$$\hat{\tau}_l - \frac{N}{2}\left(\hat{\tau}_l\hat{g}_l - \hat{g}_l^2 - \hat{\tau}_l + \hat{g}_l\right) = 0. \tag{101}$$

Equation (96), a product of functions, is Legendre transformed into a slightly less elegant form: in the case of Fourier transforms, the transform of a function product is the convolution of the respective Fourier transforms. The situation of the Legendre polynomial transform, however, is not as simple, i.e., the Wigner $3j$ symbols $\left(\begin{smallmatrix} i & j & l \\ 0 & 0 & 0 \end{smallmatrix}\right)$ are needed:

$$\hat{g}_l = (2l+1)\sum_{i=0}^{\infty}\sum_j \begin{pmatrix} i & j & l \\ 0 & 0 & 0 \end{pmatrix}^2 \hat{\kappa}_i\hat{\tau}_j. \tag{102}$$

This relation results from

$$P_{l_1}(\cos\theta)P_{l_2}(\cos\theta) = \sum_l (2l+1)\begin{pmatrix} l_1 & l_2 & l \\ 0 & 0 & 0 \end{pmatrix}^2 P_l(\cos\theta). \tag{103}$$

This solution directly yields a set of coefficients for the intercenter distribution function. The Wigner $3j$ symbols can be computed in advance using methods such as the one in [34]. Following this, the coefficients are normalized so that the PDF integral is equal to 1.

1. Approximate solution to the PY equation

To develop an approximate solution to the PY equation we begin with

$$g_N(\cos\theta) - c_N(\cos\theta) - \rho\int c_N(\cos\theta')[g_N(\vec{\Omega}'\cdot\vec{\Omega}) - 1] \times \sin\theta' d\theta' d\varphi' + \frac{1}{N} = 0 \tag{104}$$

or

$$g_N(\cos\theta) - c_N(\cos\theta) = \rho\int c_N(\cos\theta')[g_N(\vec{\Omega}'\cdot\vec{\Omega}) - 1] \times \sin\theta' d\theta' d\varphi' + 1 - \frac{1}{N}. \tag{105}$$

The PY conditions for g_N and c_N on a spherical surface are

$$g(\cos\theta) = 0, \quad \cos\theta < \cos 2\alpha_d, \tag{106}$$

$$c(\cos\theta) = 0, \quad \cos\theta > \cos 2\alpha_d. \tag{107}$$

Inserting Eqs. (106) and (107) into Eq. (105) results in the following equations:

$$-c_N(\cos\theta) = \rho\int c_N(\cos\theta')[g_N(\vec{\Omega}'\cdot\vec{\Omega}) - 1]\sin\theta' d\theta' d\varphi' + 1 - \frac{1}{N}, \quad \cos\theta > \cos 2\alpha_d \tag{108}$$

and

$$g_N(\cos\theta) = \rho\int c_N(\cos\theta')[g_N(\vec{\Omega}'\cdot\vec{\Omega}) - 1]\sin\theta' d\theta' d\varphi' + 1 - \frac{1}{N}, \quad \cos\theta > \cos 2\alpha_d. \tag{109}$$

To simplify the integration, we change the integration variables $\cos\theta = \mu$ and

$$\sin\theta d\theta d\varphi = -d\mu d\varphi. \tag{110}$$

The μ interval is discretized in a series of meshes after being partitioned into two subintervals, i.e., $[\cos 2\alpha_d, 1]$ and $[-1, \cos 2\alpha_d]$. Uniform mesh sizes are used for the two subintervals, and their sizes are chosen to be as close to each other as possible, while still allowing the boundary between these intervals to equal $\cos 2\alpha_d$. [Discontinuities in $g_N(\cos\theta)$ and $c_N(\cos\theta)$ would be poorly approximated without taking these precautions.]

A nonlinear Gauss-Seidel iteration [35] was used, where each computed value for c_N and g_N was introduced in the computation for the next mesh. To increase stability, Gauss-Seidel sweeps are done alternatively from a low to high mesh index, and from a high to low index. To prevent iteration oscillations—which may prevent convergence—ρ is increased by a constant amount for each mesh sweep, until it reaches its final value. With ρ at its final value, a number of iterations are performed until g and c converge.

2. The PY equation for a spherical surface

The exact solutions presented in the previous sections indicate that even for the case of only three domains, the mathematics can get complicated. However, in three-dimensional (3D) space one can solve the PY equation to yield a reasonable approximation for the pair correlation function. There are, however, difficulties in developing the PY equation; namely, the number of domains, N, is finite and fixed, and the surface which they occupy is finite and spherical. The first two obstacles were previously solved by White and Velasco [31] for a finite number of particles in a box by obtaining an approximate finite N form of the OZ equation. The third is tackled by considering the metric of a spherical surface as was described above; i.e.,

$$h_N(\cos\theta) = c_N(\cos\theta) + \rho \int_S h_N(\cos\theta') c_N(\vec{\Omega}\cdot\vec{\Omega}') \times \sin\theta' d\theta' d\varphi' - \frac{1}{N}. \tag{111}$$

Further,

$$h(\cos\theta) = g(\cos\theta) - 1, \tag{112}$$

$$C_{\text{full}}(\cos\theta) = 4\pi g(\cos\theta), \tag{113}$$

$$\rho = \frac{N}{4\pi}. \tag{114}$$

One can also assume that the PY conditions are true for the approximate OZ equation. Adapting it, however, requires the following conditions:

$$g(\cos\theta) = 0 \text{ or } h(\cos\theta) + 1 = 0, \quad \cos\theta < \cos 2\alpha_d, \tag{115}$$

$$c(\cos\theta) = 0, \quad \cos\theta > \cos 2\alpha_d. \tag{116}$$

There are, however, features for this system of equations that are worth investigating:

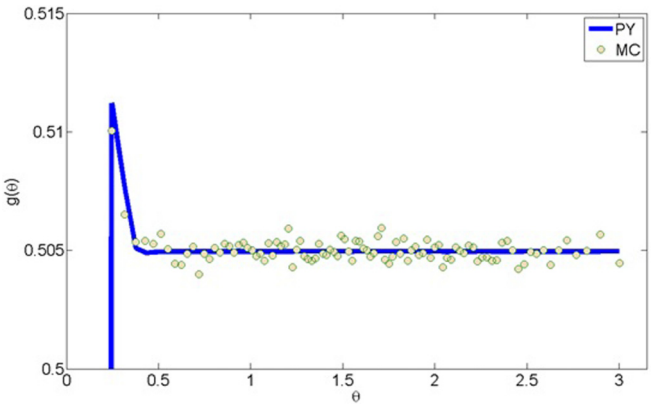

FIG. 3. Comparison of PDFs using the PY approach and MC simulations: five domains with a radial angle of 0.1 rad.

(a) To what extent is the PY approximation for the function $c(\cos\theta)$ applicable to a finite number of hard objects in a closed finite box, and are there any N-dependent terms and factors that need to be introduced, instead of the condition $c(\cos\theta) = 0$? This, however, does not seem to be the case, as the condition $c(\cos\theta)$ is local and cannot be related to the total number of domains.

(b) It may also be of interest to establish whether Eq. (93) is exactly solvable or if there are analogs for n-dimensional "spherical surfaces of radius 1" that are exactly solvable—similar to the problem in the odd n-dimensional Euclidean space [36].

Here, we compare PDFs calculated in the framework of the spherical analog of the PY approach to PDFs computed using MC simulations (see the Appendix). To check the validity of the PY approach, and its limits, we consider the case of five domains on a spherical surface. Equations (92)–(96) and Eqs. (97) and (98) were solved numerically and were found to approximate well the PDF for domain centers.

Figures 3–5 show that the PY approach of calculating PDFs is more accurate for domains with a small angular size (i.e., 0.1 rad; Fig. 3). It also implies that the PY approach for calculating PDFs of nanoscopic domains on spherical vesicles could be used to predict structures that are too small to be easily "observed" by many of the current experimental techniques. It should be noted that the agreement between the

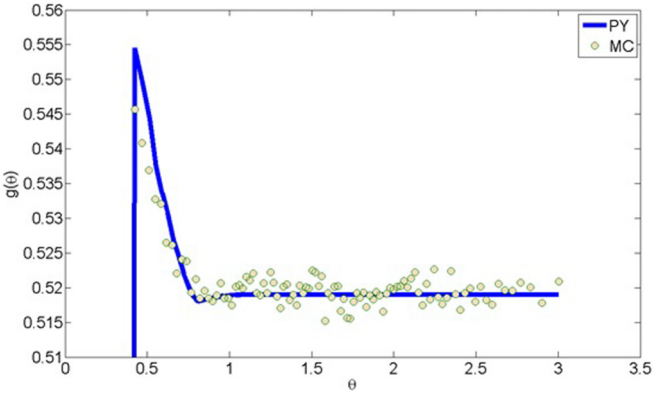

FIG. 4. Comparison of PDFs using the PY approach and MC simulations: five domains with a radial angle of 0.2 rad.

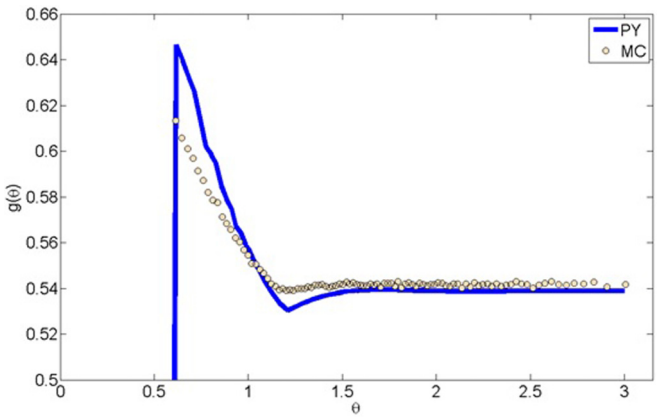

FIG. 5. Comparison of PDFs using the PY approach and MC simulations: five domains with a radial angle of 0.3 rad.

PY approach and MC simulations can be improved with the use of high-throughput computing; hence, the convergence of our MC algorithm (see the Appendix) can be enhanced.

IV. CONCLUSIONS

The analytical treatment of the scattering signal from nanoscopic domains populating a spherical vesicle is nontrivial and presents a computational challenge. Here, we described an analytical solution for calculating PDFs of same-size, randomly distributed domains on a spherical vesicle. This model can also be used for fitting scattering data of lipid vesicles with different contrast lipid and/or protein domains. For the much-studied example of circular domains on a spherical surface—commonly observed in model lipid membrane systems—intra- and interdomain correlations were treated independently. The treatment of intradomain correlations corresponds to the treatment of a form factor, while domain-domain correlations were based on a PDF analysis. Domain-domain correlations were computed analytically for two and three domains on a vesicle. The case of greater than three domains was addressed by a newly developed MC algorithm and by analogs of the OZ and PY equations, which were developed here. Importantly, the analytical solutions for intra- and interdomain correlations of randomly distributed lipid domains on vesicles offer a new approach for analyzing small-angle x-ray scattering (SAXS) and small-angle neutron scattering (SANS) data of commonly studied phase-separated model membrane systems.

In this work, we also derived analytical solutions for nanoscopic domains occupying only a small fraction of a vesicle's area using the OZ and PY frameworks. However, when the domains accounted for a significant fraction of the vesicle surface (microscopic domains), the analytical description was less than ideal. In a follow-up paper we will develop a model that includes a physical basis for domain-domain correlations.

The described PDF treatment is based purely on geometrical considerations and is in good agreement with MC simulated results. The short-range character of domain-domain correlations in lipid membranes should also be noted [37]. In the case of giant, micron-size unilamellar vesicles, and where the domain area fraction is small compared to the vesicle area, the 3D site-site PDF can be reduced to a two-dimensional analog. Therefore, using the recently developed theoretical frameworks, including exactly solvable models, one can potentially use these treatments to solve domain-domain PDFs of experimentally studied spherical vesicles [38–44]. Since the complete physical description of both intra- and interdomain correlations and lipid phase separation is still a work in progress, the applicability of alternative computational approaches to interpret experimental data should be of interest [45–50].

As mentioned, the plasma membrane, which is responsible for the permeation of molecules into the cell's interior, such as water, proteins, peptides, ions, pathogens, etc., is thought to contain lateral organization whose features range from a few to tens of nanometers. Importantly, nanoscopic lipid-protein domains are thought to be responsible for physiological functions such as transmembrane trafficking, signal transduction, and cell-cell recognition, to name a few. Despite their importance, and the many studies attempting to detect and characterize them, they have remained somewhat elusive. Recently, SANS techniques have proven capable of detecting nanoscopic domains in spherical vesicles [2] and in living bacterial cells [3]. However, due to a lack of analytical tools to interpret the scattering data, their morphologies are still not well characterized. As a result, the newly developed models presented in this paper may help us interpret scattering data in a less model-dependent manner than what has been done to date, specifically through the calculation of PDFs, structure factors, and scattering intensities.

ACKNOWLEDGMENTS

We thank Fred A. Heberle for constructive discussions and Jeremy Pencer for his careful reading of the manuscript. J.K. is supported through the Scientific User Facilities Division of the Department of Energy (DOE) Office of Science, sponsored by the Basic Energy Science (BES) Program, DOE Office of Science, under Contract No. DEAC05-00OR22725.

APPENDIX: MONTE CARLO SIMULATION TO COMPUTE DOMAIN PDFS

MC simulation was used to compute PDFs for N_d domains. To develop an effective MC method, one has to choose an appropriate set of coordinates, functions, and variables.

For the general case of identical N_d domains with circular symmetry, one starts with

$$C_{\text{full}}(\alpha,\vec{\Omega}_1\cdot\vec{\Omega}_2)=\frac{\mathrm{H}(2\alpha,\,\vec{\Omega}_1\cdot\vec{\Omega}_2)\iiint\prod_{(i,j)\neq(1,2)}\mathrm{H}(2\alpha,\,\vec{\Omega}_i\cdot\vec{\Omega}_j)d\vec{\Omega}_3d\vec{\Omega}_{4\ldots}d\vec{\Omega}_{N_d}}{\iiint\prod_{(i,j)}\mathrm{H}(2\alpha,\,\vec{\Omega}_i\cdot\vec{\Omega}_j)d\vec{\Omega}_1d\vec{\Omega}_2d\vec{\Omega}_3d\vec{\Omega}_{4\ldots}d\vec{\Omega}_{N_d}}.$$

Examining this expression, it becomes obvious that $C_{\text{full}}(\alpha, \vec{\Omega}_1 \cdot \vec{\Omega}_2)$ depends only on the radial angle α and on the vector positions of $\vec{\Omega}_1$ and $\vec{\Omega}_2$ through the sclalar product $\vec{\Omega}_1 \cdot \vec{\Omega}_2$. One then obtains

$$C_{\text{full}}(\alpha, \vec{\Omega}_1 \cdot \vec{\Omega}_2) = C_{\text{full}}(\alpha, \vec{\Omega}_i \cdot \vec{\Omega}_j).$$

Permuting indices 1 and 2 in C_{full} (i.e., 1 to i and 2 to j) allow for the equality to stand. The infinitesimal area element of the spherical surface is given by $\sin\theta d\theta\, d\varphi$, which is not uniform over θ [i.e., $\sin\theta d\theta\, d\varphi = -d(\cos\theta)d\varphi$]. This leads to a further simplification. Moreover, changing to $\mu = \cos\theta$ and changing the integration from -1 to 1 gives rise to a differential element of area $d\mu d\varphi$. Therefore, one can then use the uniformly distributed random variables μ and φ to perform the MC integration.

The PDF is computed on an interval of $\mu = \cos\theta$ within $\cos 2\alpha_d$. This interval is divided using N_{divs} points into $N_{\text{divs}} - 1$ equal meshes. N_d uniformly distributed points are generated on the surface of the unit sphere. This set of N_d points is accepted if and only if the angular distance between them is larger than $2\alpha_d$, where α_d is the radial angle of a circular domain. The N_d point set is rejected if this condition is not satisfied. Once the set is generated, the angular distances between the points are collected, increasing correspondingly the number of points that fall onto the corresponding mesh. This is a consequence of the definition of C_{full}. The process is then repeated for a new set of randomly generated points, until a sufficient number of points is accumulated and the random deviation becomes negligible.

MATLAB code implementing the simulation is available as Supplemental Material [51].

[1] C. L. Armstrong, D. Marquardt, H. Dies, N. Kučerka, Z. Yamani, T. A. Harroun, J. Katsaras, A.-C. Shi, and M. C. Rheinstädter, PLoS ONE **8**, e66162 (2013).

[2] F. A. Heberle, R. S. Petruzielo, J. Pan, P. Drazba, N. Kučerka, R. F. Standaert, G. W. Feigenson, and J. Katsaras, J. Am. Chem. Soc. **135**, 6853 (2013).

[3] J. D. Nickels, S. Chatterjee, C. B. Stanley, S. Qian, X. Cheng, D. A. A. Myles, R. F. Standaert, J. G. Elkins, and J. Katsaras, PLoS Biol. **15**, e2002214 (2017).

[4] C. M. Rosetti, A. Mangiarotti, and N. Wilke, Biochim. Biophys. Acta **1859**, 789 (2017).

[5] E. L. Talbot, L. Parolini, J. Kotar, L. Di Michele, and P. Cicuta, Proc. Natl. Acad. Sci. USA **114**, 846 (2017).

[6] S. Shikano and M. Li, Proc. Natl. Acad. Sci. USA **100**, 5783 (2003).

[7] J. T. Groves and J. Kuriyan, Nat. Struct. Mol. Biol. **17**, 659 (2010).

[8] D. W. Lee, K. Kristiansen, S. H. Donaldson, Jr., N. Cadirov, X. Banquy, and J. N. Israelachvili, Nat. Commun. **6**, 7238 (2015).

[9] J. A. Allen, R. A. Halverson-Tamboli, and M. M. Rasenick, Nat. Rev. Neurosci. **8**, 128 (2007).

[10] C. Y. Hong, C. T. Han, and L. Chao, Langmuir **32**, 6991 (2016).

[11] E. Sezgin, I. Levental, S. Mayor, and C. Eggeling, Nat. Rev. Mol. Cell Biol. **18**, 361 (2017).

[12] A. J. Sodt, R. M. Venable, E. Lyman, and R. W. Pastor, Phys. Rev. Lett. **117**, 138104 (2017).

[13] M. M. Terzi and M. Deserno, J. Chem. Phys. **147**, 084702 (2017).

[14] A. Sandoval-Perez, K. Pluhackova, and R. A. Böckmann, J. Chem. Theory Comput. **13**, 2310 (2017).

[15] M. K. Transtrum, B. B. Machta, K. S. Brown, B. C. Daniels, C. R. Myers, and J. P. Sethna, J. Chem. Phys. **143**, 010901 (2015).

[16] G. Bubnis, H. J. Risselada, and H. G. Grubmüller, Phys. Rev. Lett. **117**, 188102 (2016).

[17] A. Davtyan, M. Simunovic, and G. A. Voth, J. Chem. Phys. **147**, 044101 (2017).

[18] J. M. Falcón-González, G. Jiménez-Domínguez, I. Ortega-Blake, and M. Carrillo-Tripp, J. Chem. Theory Comput. **13**, 3388 (2017).

[19] R. Sakhardande, S. Stanojeviea, A. Baskaran, A. Baskaran, M. F. Hagan, and B. Chakraborty, Phys. Rev. E **96**, 012704 (2017).

[20] R. E. Magi and J. P. Keener, SIAM J. Appl. Math. **77**, 128 (2017).

[21] L. Xiao, J. Diao, D'Artagnan Greene, J. Wang, and R. Luo, J. Chem. Theory Comput. **13**, 3398 (2017).

[22] F. A. Heberle, V. N. P. Anghel, and J. Katsaras, J. Appl. Crystallogr. **48**, 1391 (2015).

[23] A. R. Edmonds, *Angular Momentum in Quantum Mechanics*, (Princeton University Press, Princeton, NJ,1957).

[24] V. N. P. Anghel, N. Kučerka, J. Pencer, and J.Katsaras, J. Appl. Crystallogr. **40**, 513 (2007).

[25] S. A. Rice and P. Gray, *The Statistical Mechanics of Simple Liquids* (Interscience, New York, 1965).

[26] I. Todhunter and J. G. Leathem, *Spherical Trigonometry* (Macmillan, London, 1914).

[27] J. P. Hansen and I. R. McDonald, *Theory of Simple Liquids* (Academic Press, London, 1976).

[28] F. Lado, J. Comput. Phys. **8**, 417 (1971).

[29] M. Adda-Bedia, E. Katzav, and D. Vella, J. Chem. Phys. **128**, 184508 (2008).

[30] J. K. Percus and G. J. Yevick, Phys. Rev. **110**, 1 (1957).

[31] J. A. White and S. Velasco, Europhys. Lett. **54**, 475 (2001).

[32] M. S. Wertheim, J. Mat. Phys. **5**, 643 (1984).

[33] I. N. Sneddon, *The Use of Integral Transforms* (McGraw-Hill, New York, 1972).

[34] H. T. Johansson and C. Forssén, SIAM J. Sci. Comput. **38**, A376 (2016).

[35] J. H. Mathews and K. K. Fink, *Numerical Methods Using Matlab*, 4th ed. (Prentice Hall, Upper Saddle River, NJ, 2004).

[36] E. Leutheusser, Physica A **127**, 667 (1984).

[37] R. Mukhopadhyay, K. C. Huang, and N. S.Wingreen, Biophys. J. **95**, 1034 (2008).

[38] T. Boublík, Mol. Phys. **109**, 1575 (2011).

[39] T. Boublík, Fluid Phase Equilib. **316**, 1 (2012).

[40] I. A. Zaluzhnyy, R. P. Kurta, A. P. Menushenkov, B. I. Ostrovskii, and I. A. Vartanyants, Phys. Rev. E **94**, 030701(R) (2016).

[41] P. Gurin and S. Varga, J. Chem. Phys. **139**, 244708 (2013).

[42] R. Wittmann, C. E. Sitta, F. Smallenburg, and H. Löwen, J. Chem. Phys. **147**, 134908 (2017).

[43] S. O. Yurchenko, N. P. Kryuchkov, and A. V. Ivlev, J. Phys. Condens. Matter **28**, 235401 (2016).
[44] Y. Jin, J. G. Puckett, and H. A. Makse, Phys. Rev. E **89**, 052207 (2014).
[45] D. Bolmatov, D. Zav'yalov, M. Zhernenkov, E. T. Musaev, and Y. Q. Cai, Ann. Phys. **363**, 221 (2015).
[46] T. Hoppe, PLoS ONE **8**, e75792 (2013).
[47] P. Lurie-Gregg, J. B. Schulte, and D. Roundy, Phys. Rev. E **90**, 042130 (2014).
[48] A. Z. Patashinski, R. Orlik, A. C. Mitus, M. A. Ratnera, and B. A. Grzybowski, Soft Matter **9**, 10042 (2013).
[49] M. J. Del Razo and H. Qian, Commun. Math. Sci. **14**, 1741 (2016).
[50] E. I. Kats and A. R. Muratov, Phys. Rev. E **97**, 012610 (2018).
[51] See Supplemental Material at http://link.aps.org/supplemental/10.1103/PhysRevE.97.062405 for the three MATLAB subroutines used to calculate the PDFs presented in the main body of the paper.